Generalized Plants for $\mathcal{H}_\infty$ Robust Controller Design

Koshy George,* Jang Gyu Lee,† and Bohyung Lee‡
Seoul National University,
Seoul 151-742, Republic of Korea

Introduction

ROBUSTNESS to modeling uncertainties is a vital characteristic required of any controller; a practical design technique must take into account this inadequacy of the mathematical models. Thus, robust systems must satisfy the design requirements not only for the nominal design model but for the physical system as well. The first step into designing robust systems is to build the generalized plant from the knowledge of the given plant and the weighting transfer functions that represent design objectives. The state-space realization of the generalized plant also depends on the interconnection topology. The $\mathcal{H}_\infty$ design procedure is then applied to the generalized plant to design a robust controller.

The method of $\mathcal{H}_\infty$ design generically assumes a one-degree-of-freedom configuration. Such a configuration inherently accepts two possible structures: 1) placing the controller in the forward path cascade to the given plant or 2) placing it in the feedback path. $\mathcal{H}_\infty$ robust controllers can then be computed using the standard Glover–Doyle[1] algorithm. In this Note, we compare the generalized plants obtained in these cases and show that the feedback configuration offers certain advantages that can be exploited in the design of robust controllers. The McFarlane–Glover loop shaping technique[2] is known to have many theoretical and computational benefits.[3,4] We present a feedback configuration interpretation of this method and, hence, show that the feedback configuration and the loop shaping technique have a few similar features. We then establish this similarity by designing $\mathcal{H}_\infty$ robust controllers for a satellite with flexible appendages.

Different Methods to Build the Generalized Plant

A one-degree-of-freedom controller structure typically admits the placement of the controller either in the forward path cascade to the given plant (referred to as the cascade configuration) or in the feedback path (referred to as the feedback configuration). Evidently, each configuration leads to a different generalized plant. In this section, we present state-space realizations of these generalized plants. We also provide a feedback configuration interpretation of the McFarlane–Glover loop shaping technique and its state-space realization.

The generalized plant $G(s)$ consists of the nominal model of the given plant $P(s)$, the weighting transfer functions, and the interconnection topology; let its state-space realization be as follows:

$$\dot{x}(t) = Ax(t) + B_1 w(t) + B_2 u(t) \tag{1}$$

$$z(t) = C_1 x(t) + D_{11} w(t) + D_{12} u(t) \tag{2}$$

$$y(t) = C_2 x(t) + D_{21} w(t) + D_{22} u(t) \tag{3}$$

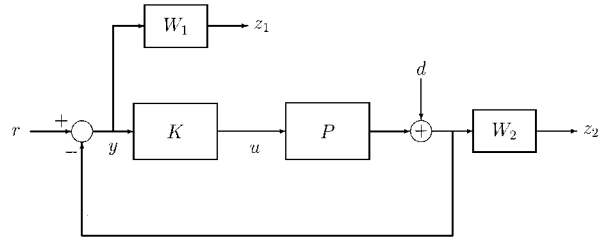

Fig. 1 Controller in the cascade position.

We design the control law $u(s) = K(s)y(s)$ such that $\|T_{zw}\|_\infty$ is minimized where T_{zw} is the closed-loop transfer function matrix from the exogenous input w to the controlled output z. We note that $w(t) \in \mathbb{R}^{m_1}$, $u(t) \in \mathbb{R}^{m_2}$, $z(t) \in \mathbb{R}^{p_1}$, and $y(t) \in \mathbb{R}^{p_2}$. We assume[1] that (A, B_2) is stabilizable, (C_2, A) is detectable, rank $D_{12} = m_2$, rank $D_{21} = p_2$, and

$$\operatorname{rank}\begin{pmatrix} A - i\omega I & B_2 \\ C_1 & D_{12} \end{pmatrix} = n + m_2, \qquad \forall \omega \in \mathbb{R}$$

$$\operatorname{rank}\begin{pmatrix} A - i\omega I & B_1 \\ C_2 & D_{21} \end{pmatrix} = n + p_2, \qquad \forall \omega \in \mathbb{R}$$

Let the given plant $P(s) = C_p(sI - A_p)^{-1}B_p + D_p$ and the weighting transfer functions $W_i(s) = \bar{C}_i(sI - \bar{A}_i)^{-1}\bar{B}_i + \bar{D}_i$, $i = 1, 2$. We denote the states of the plant and the weighting transfer functions, respectively, by x_p and $\bar{x}_i$; the input and output of the plant, respectively, by u_p and y_p. Let the number of inputs to the plant be n_i and the number of outputs from the plant be n_o.

The cascade configuration, shown in Fig. 1, is common in the literature.[5] The corresponding state-space model is as follows:

$$\begin{pmatrix} \dot{x}_p \\ \dot{\bar{x}}_1 \\ \dot{\bar{x}}_2 \end{pmatrix} = \begin{pmatrix} A_p & 0 & 0 \\ -\bar{B}_1 C_p & \bar{A}_1 & 0 \\ \bar{B}_2 C_p & 0 & \bar{A}_2 \end{pmatrix} \begin{pmatrix} x_p \\ \bar{x}_1 \\ \bar{x}_2 \end{pmatrix} + \left(\begin{array}{ccc|c} 0 & 0 & & B_p \\ \bar{B}_1 & -\bar{B}_1 & & -\bar{B}_1 D_p \\ 0 & \bar{B}_2 & & \bar{B}_2 D_p \end{array}\right) \begin{pmatrix} r \\ d \\ \hline u \end{pmatrix} \tag{4}$$

$$\begin{pmatrix} z_1 \\ z_2 \\ \hline y \end{pmatrix} = \left(\begin{array}{ccc} -\bar{D}_1 C_p & \bar{C}_1 & 0 \\ \bar{D}_2 C_p & 0 & \bar{C}_2 \\ \hline -C_p & 0 & 0 \end{array}\right) \begin{pmatrix} x_p \\ \bar{x}_1 \\ \bar{x}_2 \end{pmatrix} + \left(\begin{array}{ccc|c} \bar{D}_1 & -\bar{D}_1 & & -\bar{D}_1 D_p \\ 0 & \bar{D}_2 & & \bar{D}_2 D_p \\ \hline I & -I & & -D_p \end{array}\right) \begin{pmatrix} r \\ d \\ \hline u \end{pmatrix} \tag{5}$$

Here, the partitioning of the matrices is done appropriate to the definition of the signals associated with the generalized plant. We note that $W_1(s)$ and $W_2(s)$ are, respectively, the weights on the sensitivity $\{S_o(s) = [I + P(s)K(s)]^{-1}\}$ and complementary sensitivity $\{T_o(s) = P(s)K(s)[I + P(s)K(s)]^{-1}\}$ transfer function matrices. (The subscript o indicates that these functions are evaluated at the output of the plant.) Moreover,

$$T_{zw}(s) = \begin{Bmatrix} W_1(s)[I + P(s)K(s)]^{-1} & -W_1(s)[I + P(s)K(s)]^{-1} \\ W_2(s)P(s)K(s)[I + P(s)K(s)]^{-1} & W_2(s)[I + P(s)K(s)]^{-1} \end{Bmatrix} \tag{6}$$

Received April 27, 1998; revision received Sept. 21, 1998; accepted for publication Sept. 24, 1998. Copyright © 1998 by the American Institute of Aeronautics and Astronautics, Inc. All rights reserved.

*Postdoctoral Fellow, Automatic Control Research Center; currently Research Fellow, Systems and Control Group, Department of Electrical Engineering, Delft University of Technology, P.O. Box 5031, 2600 GA Delft, The Netherlands.
†Director, Automatic Control Research Center, and Professor, School of Electrical Engineering.
‡Doctoral Student, School of Electrical Engineering.

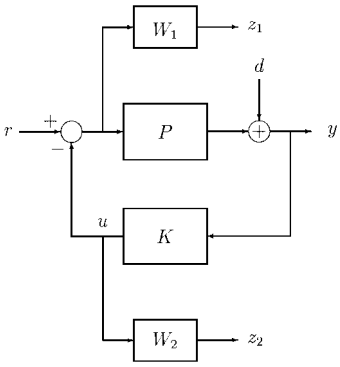

Fig. 2 Controller in the feedback position.

The feedback configuration is shown in Fig. 2, and the corresponding state-space model is as follows:

$$\begin{pmatrix} \dot{x}_p \\ \dot{\bar{x}}_1 \\ \dot{\bar{x}}_2 \end{pmatrix} = \begin{pmatrix} A_p & 0 & 0 \\ 0 & \bar{A}_1 & 0 \\ 0 & 0 & \bar{A}_2 \end{pmatrix} \begin{pmatrix} x_p \\ \bar{x}_1 \\ \bar{x}_2 \end{pmatrix} + \left(\begin{array}{cc|c} B_p & 0 & -B_p \\ \bar{B}_1 & 0 & -\bar{B}_1 \\ 0 & 0 & \bar{B}_2 \end{array}\right) \begin{pmatrix} r \\ d \\ \hline u \end{pmatrix} \tag{7}$$

$$\begin{pmatrix} z_1 \\ z_2 \\ \hline y \end{pmatrix} = \left(\begin{array}{ccc} 0 & \bar{C}_1 & 0 \\ 0 & 0 & \bar{C}_2 \\ \hline -C_p & 0 & 0 \end{array}\right) \begin{pmatrix} x_p \\ \bar{x}_1 \\ \bar{x}_2 \end{pmatrix} + \left(\begin{array}{cc|c} \bar{D}_1 & 0 & -\bar{D}_1 \\ 0 & 0 & \bar{D}_2 \\ \hline D_p & I & -D_p \end{array}\right) \begin{pmatrix} r \\ d \\ \hline u \end{pmatrix} \tag{8}$$

Evidently, $W_1(s)$ and $W_2(s)$ are, respectively, the weights on the sensitivity $(S_i(s) = [I + K(s)P(s)]^{-1})$ and the complementary sensitivity $(T_i(s) = K(s)P(s)[I + K(s)P(s)]^{-1})$ matrices. (The subscript i indicates that these matrices are computed at the input to the given plant.) Moreover,

$$T_{zw}(s) = \begin{Bmatrix} W_1(s)[I + K(s)P(s)]^{-1} & -W_1(s)[I + K(s)P(s)]^{-1}K(s) \\ W_2(s)K(s)P(s)[I + K(s)P(s)]^{-1} & W_2(s)[I + K(s)P(s)]^{-1}K(s) \end{Bmatrix} \tag{9}$$

The loop shaping procedure[2] involves preshaping the singular values of the given plant, by a precompensator W_1 and/or a postcompensator W_2, before the computation of the controller based on the normalized coprime factorization of $G(s)$. The closed-loop transfer function matrix is given by

$$T_{zw}(s) = \begin{bmatrix} W_1^{-1}(s)K(s) \\ W_2(s) \end{bmatrix} [I + P(s)K(s)]^{-1} \times \begin{bmatrix} W_2^{-1}(s) & P(s)W_1(s) \end{bmatrix} \tag{10}$$

To compare the generalized plant obtained in this case to the configurations given earlier, we note that Eq. (10) can be given a feedback configuration interpretation, as shown in Fig. 3. (We can easily show that this closed-loop transfer function matrix cannot be given a cascade configuration interpretation.) The state-space model of this system is as follows:

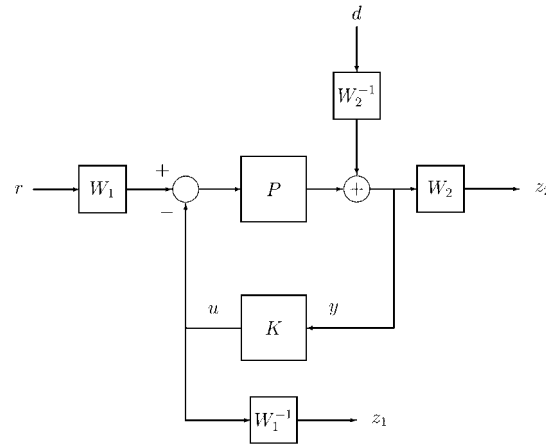

Fig. 3 Feedback configuration interpretation of the loop shaping method.

$$\begin{pmatrix} \dot{x}_p \\ \dot{\bar{x}}_1 \\ \dot{\bar{x}}_{1n} \\ \dot{\bar{x}}_2 \\ \dot{\bar{x}}_{2n} \end{pmatrix} = \begin{pmatrix} A_p & B_p\bar{C}_1 & 0 & 0 & 0 \\ 0 & \bar{A}_1 & 0 & 0 & 0 \\ 0 & 0 & \bar{A}_1 - \bar{B}_1\bar{D}_1^{-1}\bar{C}_1 & 0 & 0 \\ \bar{B}_2C_p & \bar{B}_2D_p\bar{C}_1 & 0 & \bar{A}_2 & -\bar{B}_2\bar{D}_2^{-1}\bar{C}_2 \\ 0 & 0 & 0 & 0 & \bar{A}_2 - \bar{B}_2\bar{D}_2^{-1}\bar{C}_2 \end{pmatrix} \begin{pmatrix} x_p \\ \bar{x}_1 \\ \bar{x}_{1n} \\ \bar{x}_2 \\ \bar{x}_{2n} \end{pmatrix} + \left(\begin{array}{cc|c} B_p\bar{D}_1 & 0 & -B_p \\ \bar{B}_1 & 0 & 0 \\ 0 & 0 & \bar{B}_1\bar{D}_1^{-1} \\ \bar{B}_2D_p\bar{D}_1 & \bar{B}_2\bar{D}_2^{-1} & -\bar{B}_2D_p \\ 0 & \bar{B}_2\bar{D}_2^{-1} & 0 \end{array}\right) \begin{pmatrix} r \\ d \\ \hline u \end{pmatrix} \tag{11}$$

$$\begin{pmatrix} z_2 \\ z_1 \\ \hline y \end{pmatrix} = \left(\begin{array}{ccccc} \bar{D}_2C_p & \bar{D}_2D_p\bar{C}_1 & 0 & \bar{C}_2 & -\bar{C}_2 \\ 0 & 0 & -\bar{D}_1^{-1}\bar{C}_1 & 0 & 0 \\ \hline C_p & D_p\bar{C}_1 & 0 & 0 & -\bar{D}_2^{-1}\bar{C}_2 \end{array}\right) \begin{pmatrix} x_p \\ \bar{x}_1 \\ \bar{x}_{1n} \\ \bar{x}_2 \\ \bar{x}_{2n} \end{pmatrix} + \left(\begin{array}{cc|c} \bar{D}_2D_p\bar{D}_1 & I & -\bar{D}_2D_p \\ 0 & 0 & \bar{D}_1^{-1} \\ \hline D_p\bar{D}_1 & \bar{D}_2^{-1} & -D_p \end{array}\right) \begin{pmatrix} r \\ d \\ \hline u \end{pmatrix} \tag{12}$$

Here $\bar{x}_{1n}$ and $\bar{x}_{2n}$, respectively, correspond to the states of W_1^{-1} and W_2^{-1}.

Comparison of the Generalized Plants

In this section we compare the properties of the state-space realizations of the three generalized plants presented in the preceding section. First, evidently, the generalized plant $G(s)$, in the case of cascade configuration, has a higher number of outputs than inputs $(3n_o > 2n_o + n_i)$ if the given plant $P(s)$ is tall, i.e., $n_o > n_i$, which is usually the case in practice. On the contrary, in the case of feedback configuration, $G(s)$ has at least as many inputs $(2n_i + n_o)$ as outputs $(2n_i + n_o)$; i.e., the system is square or fat.[3] This means that the generalized plant model exhibits a full row rank at all points on the imaginary axis and at infinity. Experience[6] has shown that, for reasonable sets of weighting transfer functions, meaningful controllers are easier to obtain using a fat generalized plant rather than a tall one. It frequently turns out that, in the case of tall generalized plants, the associated Riccati equations have no positive definite solutions due to numerical ill conditioning. Thus, the response of the closed-loop system is difficult to control effectively with the trial-and-error selection of weighting transfer functions. Although the loop shifting technique[7] alleviates this problem to a certain extent, we observe, in the sequel, that such a procedure can be avoided entirely in the case of the fat generalized plant obtained via the feedback configuration by a simple choice of weighting transfer functions.

Second, if $P(s)$ is strictly proper, i.e., $D_p = 0$, the assumed rank condition required for the controllers to be proper fails in the case

of cascade configuration (rank $D_{12} = 0$), and hence there is no guarantee on the realizability of the controllers. Consequently, to facilitate computation of the $\mathcal{H}_\infty$ controller, the zero D_p matrix must be replaced by a compatible matrix of small numbers[5] such that there is very little change in the behavior of the plant over the frequency range of interest. Clearly, such a problem does not exist in the case of feedback configuration.

Third, if $W_1(s)$ is chosen to be strictly proper, i.e., $\bar{D}_1 = 0$, then the matrix $D_{11} = 0$ in the case of feedback configuration. Under this condition, we can expect the value of $\|T_{zw}\|_\infty$, which is bounded below by the singular values of submatrices of D_{11}, to be lower. Further, the expressions of the Riccati equations are simpler, and hence the numerical computation is less intensive. Moreover, by examining the controller equations,[1] we conclude that an added advantage in making $D_{11} = 0$ is that the central controller is strictly proper. Such modifications cannot directly be made in the case of cascade configuration. We note that if the diagonal elements of W_1 and W_2 are, respectively, chosen as $k_1/(\tau_1 s + 1)(\tau_2 s + 1)$ and $k_2(\tau_3 s + 1)/(\tau_4 s + 1)$ then it has all of the advantages just stated, while ensuring a good roll off of the open-loop transfer function in the high-frequency ranges.

Fourth, from Eq. (9), it is evident that both multiplicative and additive uncertainties are considered in the objective function $T_{zw}(s)$; i.e., there is a weight on both complementary sensitivity function ($W_2 T_i$) and a weight on the product of the controller and the sensitivity function ($W_1 S_i K$). This is not the case with cascade configuration. Further, we can easily see that $W_1(s)$ and $W_2(s)$ are, respectively, the weights on the input sensitivity and complementary sensitivity transfer function matrices. This implies that the input multiplicative uncertainty model is used. Whereas uncertainty due to unmodeled dynamics is more appropriately described by the input multiplicative uncertainty model, the uncertainty associated with the sensors is described by the output multiplicative uncertainty model.[8] The latter model is implicitly used in the case of cascade configuration. Therefore, it is clear that the feedback configuration offers certain advantages over the cascade configuration.

As expected, the state-space model corresponding to the loop shaping procedure reveals many similarities to the properties of the feedback configuration. First, the resulting generalized plant is square. Second, there is no problem if the plant is strictly proper. Third, an observation of the first row of Eq. (10) reveals that both additive and multiplicative uncertainties are used in the model. Fourth, the input multiplicative uncertainty representation is used. However, we observe the following differences: The order of the controller is larger than that obtained by the application of the standard algorithm to the feedback configuration. This is because of the presence of the inverse of the weighting transfer functions. Further, the matrix D_{11} cannot be made zero. However, we can show that the central controller corresponding to this generalized plant is again strictly proper under mild conditions. Thus, the loop shaping technique and the feedback configuration have similar features albeit the order of the controller obtained by the former method is larger than that of the latter.

Application to a Satellite with Flexible Appendages

In this section we design two robust $\mathcal{H}_\infty$ controllers for the roll dynamics of a satellite with flexible appendages; one controller is designed using the feedback configuration and the other by directly using the loop shaping technique. The example satellite is in the class of Indian remote sensing (IRS) satellites. We assume an axisymmetric satellite with identical solar panels.

The objective of the design study is twofold: to stabilize the attitude with minimal interactions with the flexible modes of the appendages and to reject small-magnitude low-frequency disturbances that result in attitude perturbations and, hence, imprecise pointing. The IRS class satellites has a typical orbital period of 101 min, and the disturbance bandwidth is less than 0.003 rad/s. The primary requirement is to tightly control the rigid-body rates. Such requirements are met by minimizing the influence of the flexible dynamics on the satellite attitude motion.

For small motions of the satellite about its nominal operating condition, the equations for the roll dynamics of the example satellite are as follows:

$$I_{yy}\ddot{\phi} + 2b_y\ddot{q} = T_y, \qquad \ddot{q} + 2\zeta\Omega\dot{q} + \Omega^2 q + b_y\ddot{\phi} = 0 \quad (13)$$

where $I_{yy} = 1300$ N-m/s^2 is the moment of inertia of the satellite, including the solar panels, about the roll axis. Only one appendage mode ($\Omega = 4.078$ rad/s) is significantly coupled ($b_y = 21.5$) with the roll dynamics of the rigid body. The structural damping ratio ζ is 0.002. We assume that both ϕ and $\dot{\phi}$ are measured quantities. Evidently, the magnitude of the transfer function at the flexible mode is rather low.

We now build the generalized plant using the feedback configuration. The weights W_1 and W_2 are chosen to maximize the stability and performance robustness, as well as the time-domain performance. After several iterations, the following weights are chosen: $W_1(s) = 10/(1000s + 1)^2$ and $W_2(s) = 0.01(s + 1)/(0.001s + 1)$. The order of the generalized plant, and hence that of the $\mathcal{H}_\infty$ controller, is seven. We note that the controller is stable. It has one output u and two inputs ϕ and $\dot{\phi}$. These two inputs can be combined algebraically in the frequency domain resulting in a single input/single output (SISO) system from $\phi(s)$ to $u(s)$. The phase margin of this function is 132 deg, which is an ample lead. An SISO open-loop transfer function is obtained if the loop in Fig. 2 is broken at the plant input. The gain and phase margins are, respectively, 9.199 dB and 35.01 deg, indicating that the closed-loop system exhibits reasonable robustness properties.

The best that can be done for preflight evaluation of the closed-loop system is to study its time-domain performance in response to step and pulse inputs. In this Note, we consider only a step input of 0.1 deg at $d(1)$, the ϕ channel, for brevity. A detailed performance study is given in Ref. 6. The response of the closed-loop system to this input is given in Fig. 4. Evidently, the transients are brief, and the settling time of the closed-loop system is approximately 250 s (4.1% of the orbit duration). We observe that the closed-loop

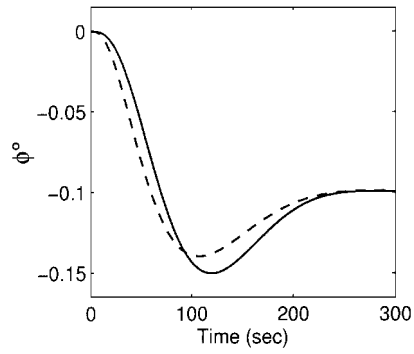

a) Roll angle

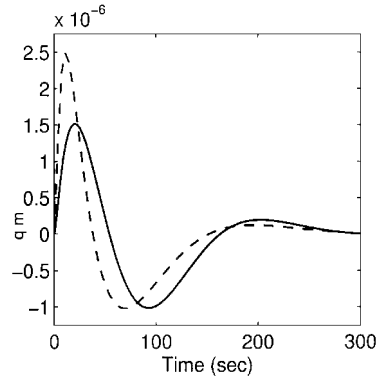

b) Modal coordinate

Fig. 4 Response of closed-loop system to a step ϕ input of 0.1 deg: ——, design using feedback configuration, and – – –, design using loop shaping technique.

system is able to track step inputs at $d(1)$. [We note that with a zero r input (Fig. 2), the output $y_p(s)$ of the plant $P(s)$ is given by $-P(s)K(s)[I + P(s)K(s)]^{-1}d(s)$; thus, in the steady state, the component of $y_p(t)$ corresponding to $\phi(t)$ goes to -0.1 deg in response to the positive step input of 0.1 deg at $d(1)$.] We note that the effect of this input to the body rate is low, and the interactions between the rigid-body dynamics and the flexible dynamics are rather low; the rigid-body dynamics continue to influence the flexible body dynamics more than vice versa. This is evident from the response plots of the flexible mode shown in Fig. 4: the overall shape of these curves are similar to those of the rigid-body rate response curves.

We now design a controller using the loop shaping technique. After several iterations we choose the following weighting transfer functions: $W_1(s) = 1/(s+1)$ and $W_2(s) = I$. The order of the controller is, therefore, six. We note that the response of the closed-loop system to a step input of 0.1 deg at the ϕ channel is similar to that of the earlier design. We observe a little increase in the deflection of the flexible mode and its rate (not shown).

The effect of controller order reduction is evaluated next. In both cases, the order can be reduced to three with very little change in the robustness properties or the time-domain performance of the closed-loop system with reduced-order controllers. Moreover, a perturbation of 30% in the natural frequency and 15% in the coupling coefficients of the flexible modes is observed to have no effect on the robustness of the closed-loop system and the time-domain performance for the first design; a slight deterioration in the response of the flexible mode is observed. For brevity, the response plots are not included. Thus, the controllers obtained by the feedback configuration and the loop shaping technique have many common characteristics and yield similar closed-loop responses.

Conclusions

We presented different ways to build the generalized plant. We showed that the feedback configuration has certain advantages over the cascade configuration, which can usefully be employed while computing the $\mathcal{H}_\infty$ robust controller by the Glover–Doyle algorithm. By providing a feedback configuration interpretation of the McFarlane–Glover loop shaping technique, we conclude that it has characteristics similar to that of the feedback configuration. We then establish this by showing that the robust controllers designed to control the roll dynamics of a satellite with flexible appendages generates closed-loop systems that have similar robustness properties and time-domain performance.

References

[1]Glover, K., and Doyle, J. C., "State-Space Formulae for All Stabilizing Controllers that Satisfy an H_∞ Norm Bound and Relations to Risk Sensitivity," *Systems and Control Letters*, Vol. 11, No. 3, 1988, pp. 167–172.

[2]McFarlane, D. C., and Glover, K., *Robust Controller Design Using Normalized Coprime Factor Plant Descriptions*, Vol. 138, Lecture Notes in Control and Information Sciences, Springer–Verlag, Berlin, 1990, Chap. 6.

[3]Vidyasagar, M., *Control System Synthesis: A Factorization Approach*, MIT Press, Cambridge, MA, 1985, Chap. 6.

[4]McFarlane, D., Glover, K., and Vidyasagar, M., "Reduced-Order Controller Design Using Coprime Factor Model Reduction," *IEEE Transactions on Automatic Control*, Vol. 35, No. 3, 1990, pp. 369–373.

[5]Maciejowski, J. M., *Multivariable Feedback Design*, Addison–Wesley, Wokingham, England, UK, 1989, Chap. 6.

[6]George, K. K., "$\mathcal{H}_\infty$-Based Robust Controller for Aerospace Vehicles," Ph.D. Thesis, Dept. of Aerospace Engineering, Indian Inst. of Science, Bangalore, India, Nov. 1996.

[7]Safonov, M. G., Limebeer, D. J. N., and Chiang, R. Y., "Simplifying the H^∞ Theory via Loop-Shifting, Matrix-Pencil and Descriptor Concepts," *International Journal of Control*, Vol. 50, No. 6, 1989, pp. 2467–2488.

[8]Freudenberg, J. S., and Looze, D. P., *Frequency Domain Properties of Scalar and Multivariable Feedback Systems*, Vol. 104, Lecture Notes in Control and Information Sciences, Springer–Verlag, Berlin, 1988, Chap. 5.

Efficient, Near-Optimal Control Allocation

Wayne C. Durham*
Virginia Polytechnic Institute and State University, Blacksburg, Virginia 24061-0203

Introduction

WE address the problem of allocating several redundant control effectors in the generation of specified body-axis moments. The effectors are constrained by position limits and are assumed to be linear in their effectiveness. The optimal solution to this problem in terms of generating maximum attainable moments for admissible controls was previously addressed in Refs. 1–3. The computational complexity of the algorithm developed in Ref. 2 to obtain such solutions is proportional to the square of the number of controls, which could become problematic in real-time applications. Other methods that generate solutions for maximum attainable moments, e.g., null-space intersections,[4,5] are even more computationally complex. This Note describes a computationally simple and efficient method to obtain near-optimal solutions. The method is based on prior knowledge of the controls' effectiveness and limits and on precalculation of several generalized inverses based on those data.

Nature of the Problem

For m controls $\boldsymbol{u}$ with effectiveness B in producing moments $\boldsymbol{m}$, the allocation problem is an underdetermined system of linear equations $\boldsymbol{m} = B\boldsymbol{u}$ with admissible controls $\boldsymbol{u} \in \Omega$, $\Omega = \{\boldsymbol{u} \mid u_i \geq u_{i,\min}, u_i \leq u_{i,\max}\}$, $i = 1, \ldots, m$. The admissible controls map to the attainable moments Φ where $\Phi = \{\boldsymbol{m} \mid \boldsymbol{m} = B\boldsymbol{u}, \boldsymbol{u} \in \Omega\}$. The attainable moments in Φ are bounded by a polyhedron whose boundary consists of parallelograms (the facets), each associated with a pair of controls. The maximum attainable desired moment $\boldsymbol{m}_d$ in some arbitrary direction occurs at the intersection of a line in the same direction as $\boldsymbol{m}_d$ with a facet on the convex hull. The determination of the proper facet requires a search that terminates when the proper facet is found: There is no assurance that this will not be the last facet tested.

The reason for the requirement to search the facets is that there is no simple way to relate a direction in moment space to the four directions that define the vertices of a particular facet. As a result, the facets must be individually tested. There are several ways in which the search order may be prioritized that will reduce the average search time, but none of these methods ensure that the worst case (in which the correct facet is the last one examined) will not often occur. In real-time applications, the frequently occurring worst case may drive the timing budgeted for control allocation.

Approximating Φ

The ideal facets of Φ, if such existed, would be those for which simple tests could be applied to $\boldsymbol{m}_d$ to determine the facet toward which it points and for which a subsequent closed-form solution to the allocation problem existed. Therefore, we seek to approximate the polyhedron that is Φ with another polyhedron whose facets satisfy this ideal requirement. We begin by constructing such a polyhedron, then determine the closed-form solutions associated with its facets.

Sectors of Moment Space

The simplest tests are relational among and between the three components of $\boldsymbol{m}_d$. Each component may be tested for sign, and the relative magnitudes of the three components established. The sign of each of the three components serves to determine the orthant (a

Received June 29, 1998; revision received Sept. 3, 1998; accepted for publication Sept. 15, 1998. Copyright © 1998 by Wayne C. Durham. Published by the American Institute of Aeronautics and Astronautics, Inc., with permission.

*Associate Professor, Department of Aerospace and Ocean Engineering. Senior Member AIAA.